Article

Electrically Rotatable Polarizer Using One-Dimensional Photonic Crystal with a Nematic Liquid Crystal Defect Layer

Ryotaro Ozaki [1,*], Masanori Ozaki [2] and Katsumi Yoshino [3]

[1] Graduate School of Science and Engineering, Ehime University, 3 Bunkyo-Cho, Matsuyama, Ehime 790-8577, Japan

[2] Division of Electrical, Electronic and Information Engineering, Graduate School of Engineering, Osaka University, 2-1 Yamada-oka, Suita, Osaka 565-0871, Japan; E-Mail: ozaki@eei.eng.osaka-u.ac.jp

[3] Shimane Institute for Industrial Technology, Matsue, Shimane 690-0816, Japan; E-Mail: yoshino@shimane-iit.jp

* Author to whom correspondence should be addressed; E-Mail: ozaki.ryotaro.mx@ehime-u.ac.jp; Tel.: +81-89-927-9764; Fax: +81-89-927-9790.

Academic Editor: Oleg D. Lavrentovich

Abstract: Polarization characteristics of defect mode peaks in a one-dimensional (1D) photonic crystal (PC) with a nematic liquid crystal (NLC) defect layer have been investigated. Two different polarized defect modes are observed in a stop band. One group of defect modes is polarized along the long molecular axis of the NLC, whereas another group is polarized along its short axis. Polarizations of the defect modes can be tuned by field-induced in-plane reorientation of the NLC in the defect layer. The polarization properties of the 1D PC with the NLC defect layer is also investigated by the finite difference time domain (FDTD) simulation.

Keywords: liquid crystal; photonic crystal; polarization

1. Introduction

Photonic crystals (PCs) are one-dimensional (1D), two-dimensional (2D), or three-dimensional (3D) ordered structures with a periodicity comparable to an optical wavelength. They are composed of two or more different dielectrics and their periodicity opens up a photonic band gap (PBG) in which the

existence of photons is forbidden [1,2]. This can be explained by an analogy of electrons in a solid-state crystal. In a PBG, electromagnetic fields cannot propagate due to destructive interference between waves scattered from the periodically modulated refractive index structure. This fact is similar to the destructive interference of electron waves from a periodic potential of an atomic lattice in a certain frequency. PCs have attracted considerable attention from both fundamental and practical points of view because various applications of PCs have been proposed [3–7].

Tunable PCs have been proposed by using opals or inverse opals infiltrated with liquid crystal (LC) having optical anisotropy and field sensitivity [8–12]. LCs are mesophases between crystalline solids and isotropic liquids. They may flow like viscous fluids and also possess features that are characteristic of solid crystals. The constituents are rod-like or disk-like organic molecules which normally have self-assembled characteristics. These molecules exhibit different physical properties between the long and short molecular axes. Consequently, LCs have various anisotropies, such as permittivity, refractive index, and viscosity. We can control the molecular director by application of an electric field because the fluidity and dielectric anisotropy allow LC molecules to align parallel or perpendicular to the electric field. Such a change of molecular orientation allows us to control the optical properties of a LC-filled PC because optical properties of PCs are determined by refractive index modification.

When there is a defect that disturbs the periodicity of a PC, localized photonic states appear in a PBG. The states are so-called defect modes at which photons are confined in the defect. In particular, 3D PBG materials with a defect allow us to achieve a 3D photon confinement. Such an optical confinement is the most important feature of PCs because an electric field in a defect can be strongly enhanced at a defect mode resonance frequency. An appropriate line defect in a 2D or 3D PC serves as a waveguide that can guide light in a desired direction by PBG confinement [13,14]. Such a defect acting as a microcavity or a waveguide is very important in certain applications, such as low-threshold lasers, micro-waveguides, and optical circuits [13–19].

Tunable defect modes are also an attractive subject. However, the introduction of a defect in a 3D PC using a nano-fabrication remains a major technical challenge [14]. Although 1D PCs do not have a complete PBG, there are plenty of applications using an extraordinary wavelength dispersion and a localized photonic state in a defect layer. So far, intensive studies on 1D PC applications have been reported: air-bridge microcavities [20,21], photonic band-edge lasers [17], nonlinear optical diodes [22], and enhancements of optical nonlinearity [23,24]. We have studied a nematic LC (NLC) layer in a dielectric multilayer as a defect in a 1D PC [25–28], in which the wavelengths of defect modes were controlled upon applying an electric field based on a change in the optical length of the defect layer caused by field-induced molecular reorientation of the NLC. Furthermore, the modulation of defect mode lasing [25] and the high speed electrooptic switching [26,27] upon applying a low voltage have been demonstrated by using a 1D PC containing an NLC defect layer. Recently, some interesting concepts have been reported using various LC defects in a 1D PC [29–32]. In this paper, we investigate polarization characteristics of defect mode peaks in a 1D PC with an NLC defect. The polarization control at the defect mode wavelength is demonstrated by in-plane reorientation of the NLC defect layer. Furthermore, the finite difference time domain (FDTD) simulation is also performed to investigate the polarization of transmitted light from the 1D PC with the NLC defect.

2. Experimental

A schematic view of a 1D PC with an in-plane NLC defect is shown in Figure 1. A dielectric multilayer as a 1D PC consisted of an alternative stack of SiO_2 and TiO_2 layers deposited on a glass substrate. The refractive indices of SiO_2 and TiO_2 are 1.46 and 2.35, respectively. The number of SiO_2-TiO_2 pairs on each substrate was five and the center wavelength of the photonic band was adjusted to be 600 nm. To obtain the 600 nm center wavelength, the thicknesses of SiO_2 and TiO_2 layers were set to be 103 and 64 nm, respectively. NLC (Merck, E44) was sandwiched between two dielectric multilayers with 1 μm spacers. The ordinary and extraordinary refractive indices of the NLC at room temperature are 1.53 and 1.78, respectively, and the dielectric anisotropy $\Delta\varepsilon$ is positive. To avoid an azimuthal anchoring effect on the surface, the top surface of the dielectric multilayer was coated with a polyimide (JSR Corporation, JALS-2021-R2, Tokyo, Japan) as a homeotropic alignment layer. In absence of an electric field, the NLC molecules aligned perpendicular to the substrate.

Six electrodes were used to control the direction of the NLC in the defect layer, as shown in Figure 1. The electrodes were fabricated by deposition of Cr and Au on the top surface of the dielectric multilayer. Thicknesses of Cr and Au electrodes were 20 and 50 nm, respectively. The width of the electrode was 25 μm and the distance of the opposite electrode was 100 μm. Using these electrodes, we were able to apply an electric field parallel to the surface (the *xy*-plane) and were able to change the direction of the field. A rectangular wave voltage of 1 kHz was applied between the six electrodes to change the molecular orientation of the NLC in the defect layer. We observed the reorientation of the NLC molecules with a polarization microscope (Nikon, ECLIPSE E600POL, Tokyo, Japan). Transmission spectra of the 1D PC with the NLC defect were measured by a charge-coupled device (CCD) multichannel spectrometer (Hamamatsu Photonics, PMA-11, Hamamatsu, Japan) attached to the polarization microscope. The numerical aperture and magnification of the objective lens were 0.45 and 50, respectively. Unpolarized or circularly polarized incident light is suitable for polarization analysis. In this experiment, circularly polarized light was entered to the device to ensure directional independence of polarization, as shown in Figure 1.
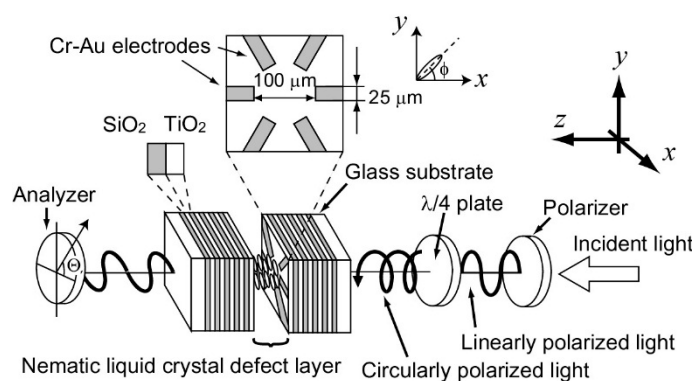

Figure 1. Experimental set-up and a schematic view of a 1D PC with a NLC defect layer.

3. Results and Discussion

Polarization microscope images of the NLC defect layer are shown in Figure 2a–c, where we used the circuits to apply a voltage to the six electrodes. The angle Φ represents the direction of an applied

electric field. Under no electric field, the NLC molecules in the defect layer aligned homeotropically because the NLC layer at 0 V was always dark despite rotating the cell on the microscope stage. In Figure 2a–c, a rectangular wave voltage of 200 V with a frequency of 1 kHz was applied between hatched and non-hatched electrodes. In this system, Φ can be controlled by adjusting positions of the potential applied to six electrodes. When the electric field was applied along Φ = 0° as shown in Figure 2a, the NLC director aligned parallel to Φ = 0°. Under the condition, the NLC at the center of the electrodes was in a dark state because the NLC director was parallel to the analyzer. In contrast, in Figure 2b,c, the NLC aligned along Φ = 60° and Φ = 120°, and then a bright state was obtained. From these results, we confirmed that the NLC director in the defect layer was able to be electrically controlled.
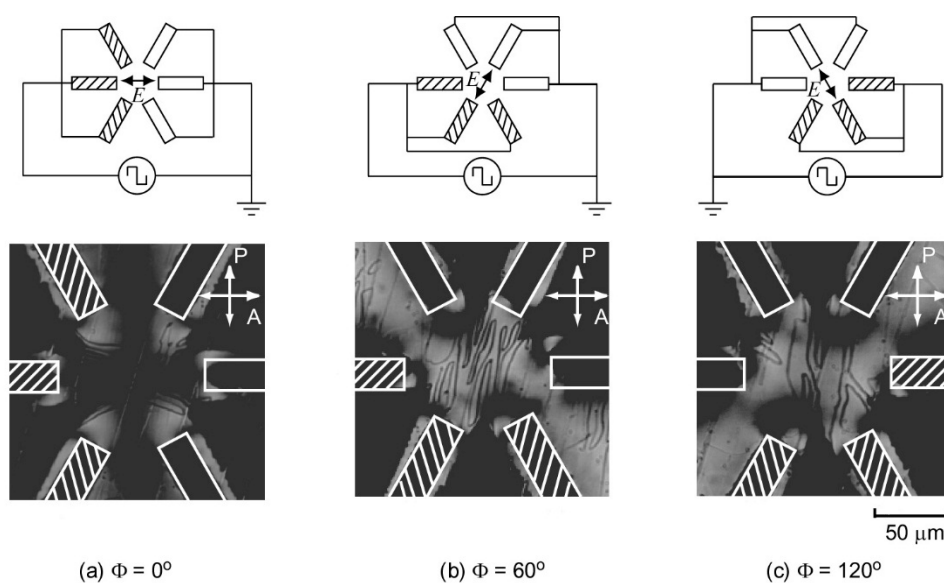

(a) Φ = 0°   (b) Φ = 60°   (c) Φ = 120°

Figure 2. Polarization microscopic images of the NLC defect layer upon applied electric field for (**a**) Φ = 0°, (**b**) Φ = 60°, and (**c**) Φ = 120°. Illustrated circuits were used to apply a voltage to the six electrodes.

Furthermore, we also performed a numerical calculation of an electric field in the defect layer using a finite differential method to investigate details of NLC directors. In this calculation, the calculated area of the defect layer was composed of 100 × 100 grid alignments. Since the electric field was mainly applied to the center of six electrodes, the potential of the boundary far away from electrodes was set to be zero. To obtain potentials at all grids, we numerically solved Laplace's equation using an iterative method. Figure 3a shows the calculated potential profile when a rectangular wave voltage of 200 V was applied between hatched and non-hatched electrodes shown in Figure 2a. Here, the potential profile shows only the center area. The calculated electric field vectors are shown in Figure 3b in which arrow size and direction represent the magnitude and the direction of the electric field, respectively. We here consider that NLC directors align parallel to arrows because Δε is positive. Under a crossed Nicols condition, when NLC directors are parallel to the polarizer or analyzer, a dark state is obtained in a polarization microscopic image. Note that arrows parallel to the polarizer or analyzer correspond to dark states in Figure 2a. In contrast, arrows not parallel to the polarizer or analyzer correspond to bright states. These calculations explain the experimental result shown in Figure 2a. Therefore, the orientation of the NLC in the defect layer was also confirmed theoretically.
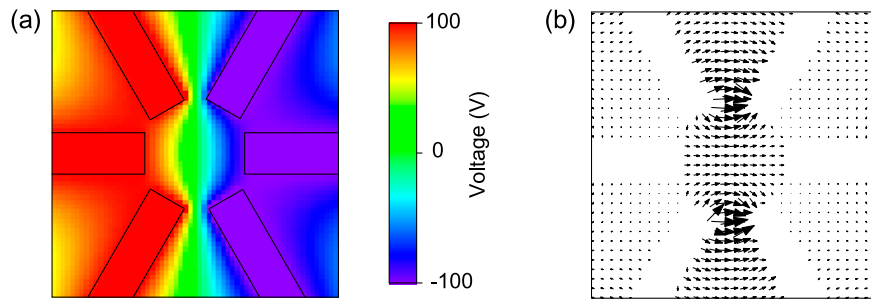
Figure 3. (**a**) Calculated potential in the NLC defect layer obtained by applying a rectangular voltage of 200 V with $\Phi = 0°$; (**b**) Calculated electric field vectors in the NLC defect layer.

We measured transmission spectra of the 1D PC with the NLC defect after the polarization microscopic observations. Incident light was circularly polarized and was obtained by placing a λ/4 plate after the polarizer, as shown in Figure 1. To investigate polarization characteristics of transmitted light, the analyzer was rotated in the transmission measurements. Figure 4 shows transmission spectra of the 1D PC with the NLC defect at $\Phi = 0°$ as a function of analyzer angle Θ.
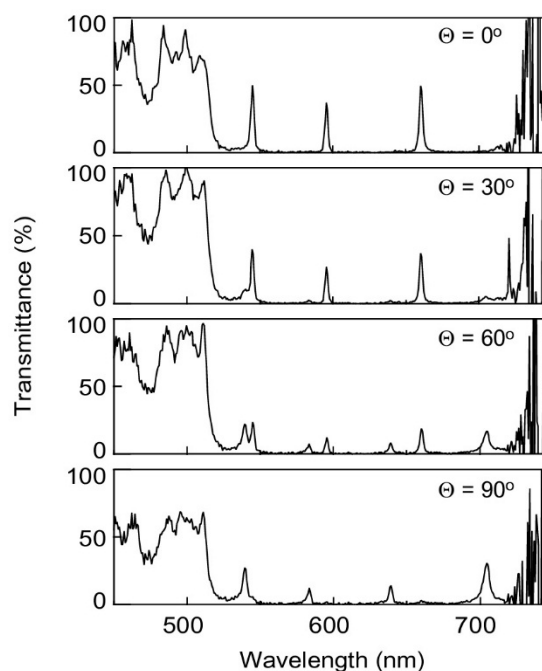

Figure 4. Transmission spectra of the 1D PC with the NLC defect for analyzer angles: $\Theta = 0°$, 30°, 60°, and 90°.

Note that some peaks appeared in the PBG of the 1D PC which were observed in the spectral range from 530 to 750 nm. These peaks were caused by defect modes induced by the introduction of the NLC defect layer. It is clear that intensities of the defect mode peaks depend on Θ. At $\Theta = 0°$, three peaks appeared at 545, 595, and 660 nm. The peak intensities decreased with the rotating analyzer from $\Theta = 0°$ to 90°, and then another four peaks at 540, 583, 640, and 705 nm appeared in the PBG. Regardless of entering circularly polarized light, intensities of the transmitted lights propagating through the 1D PC

with the NLC defect depended on Θ. These results indicate that transmitted lights at defect mode wavelengths are polarized to a certain direction.

To investigate the details of the polarization characteristics, we plotted peak intensities of the defect modes. Figure 5 shows polarization characteristics of the transmitted light through the 1D PC with the NLC defect for $\Phi = 0°$, 60°, and 90°. Red and black broken lines are $\sin^2(\Theta - \Phi)$ and $\cos^2(\Theta - \Phi)$, respectively, and the experimental data fits the curves well. Note that the maximum values of defect mode peaks for 595 and 583 nm approximately appear at $\Theta = \Phi$ and $\Theta = \Phi + 90°$, respectively. This means that transmitted lights at defect mode wavelengths are polarized along the long or short axis of the NLC molecules. In other words, the defect modes are associated with the extraordinary and ordinary refractive indices of the NLC molecules in the defect layer. The phenomenon can be explained as follows. The incident light induces a dipole moment along the short and the long molecular axes. The dipole moment is the origin of the polarization of light. In a PBG, dipole radiation is suppressed, except at a defect mode wavelength. Optical conditions for forming a defect mode are different between ordinary and extraordinary modes. Therefore, the transmitted light at a defect mode wavelength will have a linear polarization parallel to the short or the long molecular axis. Figure 5 also indicates that the polarization of the transmitted light can be controlled by changing the applied electric field direction. On the other hand, it is demonstrated from the theoretical calculation that the electric field in the defect layer can be controlled in any direction upon arranging the distribution of an applied voltage to the electrodes. Figure 6 shows calculated potentials and electric fields in the defect layer when three-phase AC voltage (three phases A, B, and C) are applied. Figure 6a,d are snapshots of the potential of the three-phase AC voltage at phase A = 0° and its electric field, respectively. The electric field vectors at the center of the six electrodes were parallel to the *x*-axis. In contrast, the electric field vectors at the center area in Figure 6e orient with an angle of 45° from the *x*-axis. The difference between Figure 6d,e is caused by the phase angle of the voltage. Similarly, Figure 6f shows electric field vectors parallel to the *y*-axis at the center area. From these results, we consider that the 1D PC with the NLC defect is expected to be a candidate for an optical rotator [33–35].
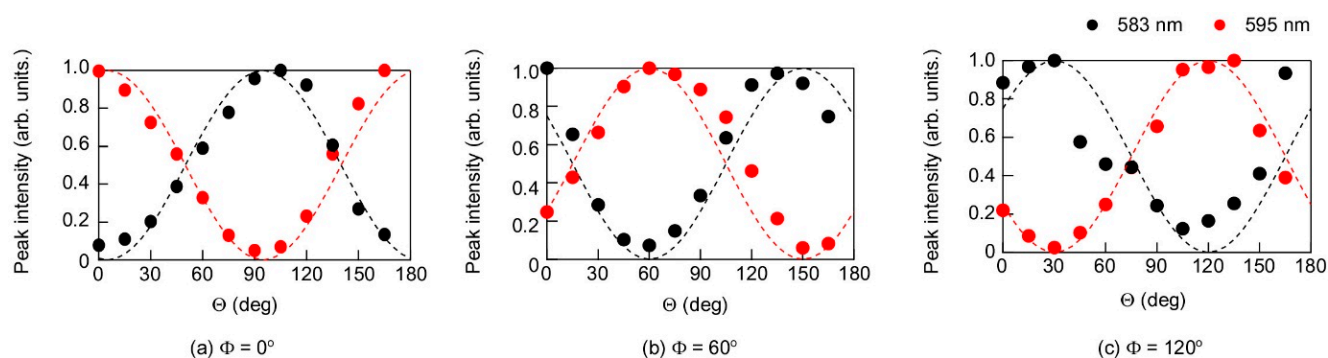

Figure 5. Polarization characteristics of the defect mode peaks at 583 and 595 nm in the 1D PC with the NLC defect for three applied electric field directions: (**a**) $\Phi = 0°$, (**b**) $\Phi = 60°$, and (**c**) $\Phi = 120°$.
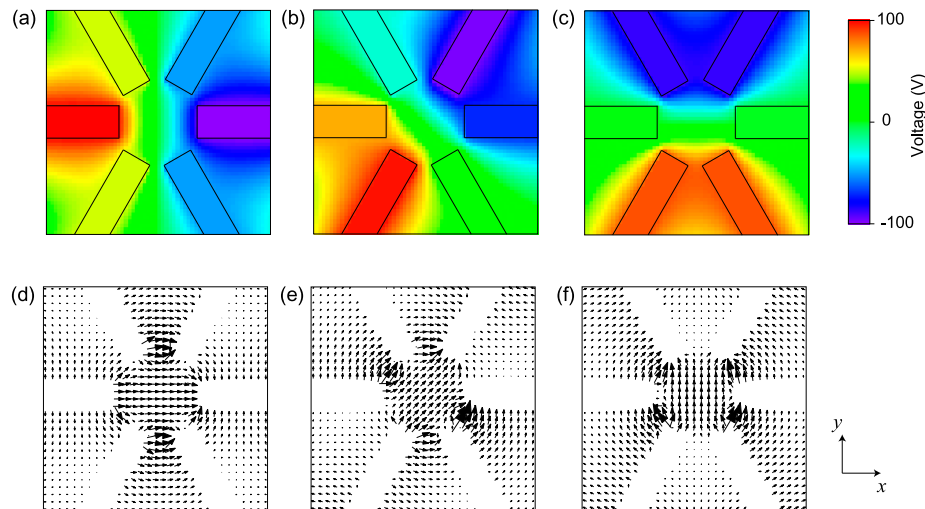
Figure 6. Snapshots of calculated potential in the NLC defect layer obtained by applying three-phase AC voltage: (**a**) Phase A = 0°, (**b**) Phase A = 45°, and (**c**) Phase A = 90°. Calculated electric field vectors at (**d**) Phase A = 0°, (**e**) Phase A = 45°, and (**f**) Phase A = 90°.

We also performed numerical calculations of the light propagation through the 1D PC with the NLC defect using the FDTD method. The FDTD calculation is an analysis of the Maxwell equations according to the Yee algorithm in discrete time and lattices [36]. Figure 7a shows the profile of ε_{xx} of the 1D PC with the NLC defect at $\phi = 0°$, where ϕ is an azimuthal angle of the NLC molecules in the defect layer as shown in Figure 1.
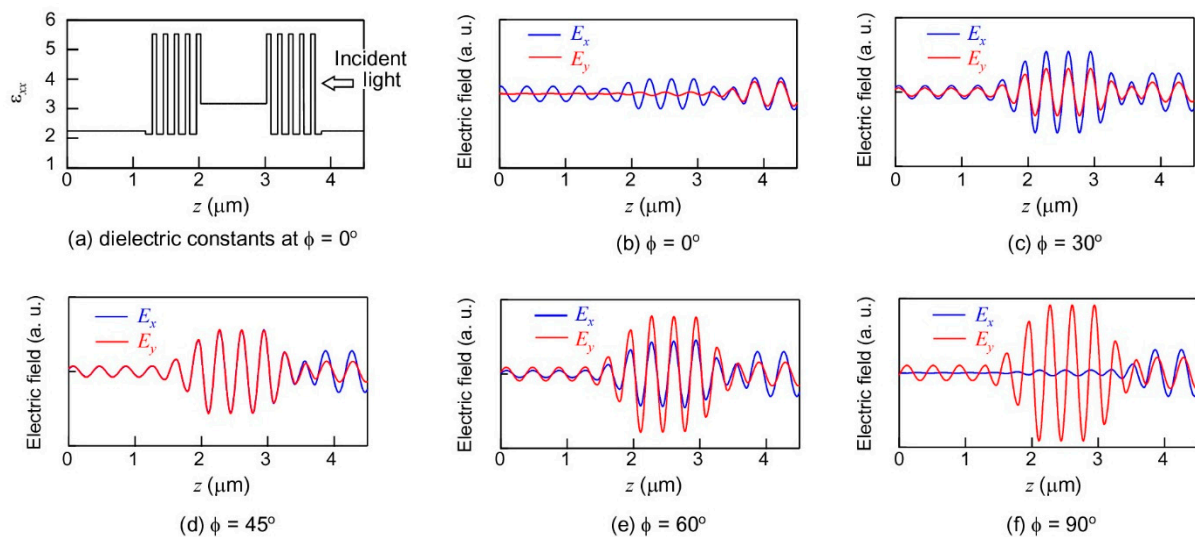

Figure 7. Calculated structure of the 1D PC with the NLC defect: (**a**) ε_{xx} profile at $\phi = 0°$. Electric field profiles of E_x and E_y propagating through the 1D PC with the NLC defect at a wavelength of 595 nm: (**b**) $\phi = 0°$, (**c**) $\phi = 30°$, (**d**) $\phi = 45°$, (**e**) $\phi = 60°$, and (**f**) $\phi = 90°$.

We used physical parameters of this structure described in Section 2. In this calculation, the circularly polarized light with a wavelength of 595 nm was entered to the 1D PC with the NLC defect along the *z*-axis, and the NLC defect layer was placed in the region from $z = 2$ to 3 μm. The first-order Mur's absorbing boundary condition was used at the boundaries of the system. Figure 7b–f shows electric field profiles

of E_x and E_y propagating through the 1D PC with the NLC defect. The polarization of transmitted light can be estimated from the difference between E_x and E_y at the output side. In Figure 7b, E_x propagates through the 1D PC with the NLC defect, whereas E_y is hardly transmitted. When the NLC director aligns to $\phi = 45°$, amplitudes of E_x and E_y become equal as shown in Figure 7d. At $\phi = 90°$, E_x is hardly transmitted, whereas E_y propagates through the 1D PC with the NLC defect. Another important fact is that E_x and E_y are almost in phase. This indicates that the polarization of the transmitted light from the 1D PC with NLC defect is linear.

Let us see the calculated transmitted light from a different angle. Figure 8a shows calculated polarization characteristics of the transmitted light propagating through the 1D PC with the NLC defect. In this graph, the transmitted E_x and E_y are plotted in the *xy*-plane. Note that the polarizations of the transmitted light are varied by rotating NLC molecules in the defect. Furthermore, the polarization angles agree with ϕ. However, the calculated transmitted light polarization is shown a little bit elliptically. Ellipticity defined by the elliptic short axis divided by the long axis is 0.04. In this case, the polarization extinction ratio at the wavelength is 625:1. This result is caused by the fact that the ten-period 1D PC does not have enough periodicity to forbid other components. Figure 8b shows the polarization of the 16-period 1D PC with the NLC defect which has stronger suppression in the PBG. As is evident from this figure, characteristics of the polarization propagating through the 16-period 1D PC with the NLC defect are sharper. Ellipticity of the 16-period 1D PC with the NLC defect is 0.01, and the polarization extinction ratio becomes 10000:1. The output polarizations of $\phi = 0°$ and $\phi = 90°$ are not exactly vertical or horizontal. This is because transmitted light and leaked light are not in phase. From the FDTD calculations we found that the polarization of transmitted light from the system was linear and parallel to ϕ and that the linearity depends on the number of periods of the 1D PC.
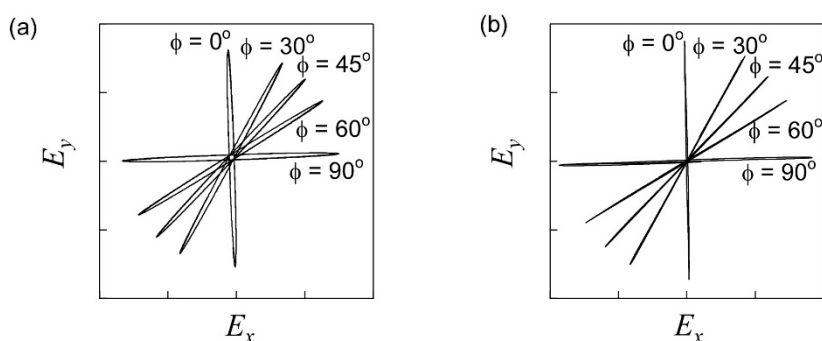

Figure 8. Calculated transmitted light propagating through the 1D PC with the NLC defect at a wavelength of 595 nm as a function of ϕ. The numbers of periods of 1D PC are (**a**) 10 and (**b**) 16.

4. Conclusions

We investigated the polarization characteristics of the transmitted light at the defect mode wavelength in the 1D PC with the NLC defect. Transmitted lights at defect mode wavelengths were polarized along the long or short axis of NLC molecules. We also demonstrated that the polarization angle at the defect mode could be controlled by field-induced in-plane realignment of the NLC molecules. To investigate details of NLC directors, numerical calculations were performed using the finite differential method.

The calculated electric field profiles explained the polarized microscopic texture of the NLC in the defect layer. These theoretical calculations showed that the electric field in the defect layer was able to control any direction upon arranging the distribution of the applied voltage to the electrodes. Furthermore, the polarization characteristics of transmitted light at a defect mode wavelength were investigated using FDTD calculations. Linearity and sharpness of the transmitted light polarization depended on the number of layers of the 1D PC. Although the measured polarization had a few percents of wrong polarization components, FDTD calculations indicated that this device still has a room for improvement in polarization property. In the experiment, some defect mode peaks had a maximum transmittance of approximately 50%. This is a good performance because 50% is the maximum transmission for a polarizer. The aperture of the device is small at the present stage, and enlargement of the aperture is the subject of further study. We expect that the LC device will find newer applications such as a high-speed electrically controllable polarization rotator.

Author Contributions

Ryotaro Ozaki carried out the measurements and analysis, and wrote the manuscript. Masanori Ozaki designed the study and discussed the experimental data and calculations. Katsumi Yoshino supervised the project.

Conflicts of Interest

The authors declare no conflict of interest.

References

1. Yablonovitch, E. Inhibited spontaneous emission in solid-state physics and electronics. *Phys. Rev. Lett.* **1987**, *58*, 2059–2062.
2. John, S. Strong localization of photons in certain disordered dielectric superlattices. *Phys. Rev. Lett.* **1987**, *58*, 2486–2489.
3. Joannopoulos, J.D.; Villeneuve, P.R.; Fan, S. Photonic crystals: Putting a new twist on light. *Nature* **1997**, *386*, 143–149.
4. Russell, P. Photonic crystal fibers. *Science* **2003**, *299*, 358–362.
5. Soljačić, M.; Joannopoulos, J.D. Enhancement of nonlinear effects using photonic crystals. *Nature Mater.* **2004**, *3*, 211–219.
6. Noda, S.; Fujita, M.; Asano, T. Spontaneous-emission control by photonic crystals and nanocavities. *Nature Photon.* **2007**, *1*, 449–458.
7. Baba, T. Slow light in photonic crystals. *Nature Photon.* **2008**, *2*, 465–473.
8. Yoshino, K.; Shimoda, Y.; Kawagishi, Y.; Nakayama, K.; Ozaki, M. Temperature tuning of the stop band in transmission spectra of liquid-crystal infiltrated synthetic opal as tunable photonic crystal. *Appl. Phys. Lett.* **1999**, *75*, 932–934.
9. Busch, K.; John, S. Liquid-crystal photonic-band-gap materials: The tunable electromagnetic vacuum. *Phys. Rev. Lett.* **1999**, *83*, 967–970.

10. Shimoda, Y.; Ozaki, M.; Yoshino, K. Electric field tuning of a stop band in a reflection spectrum of synthetic opal infiltrated with nematic liquid crystal. *Appl. Phys. Lett.* **2001**, *79*, 3627–3629.

11. Kang, D.; Maclennan, J.E.; Clark, N.A.; Zakhidov, A.A.; Baughman, R.H. Electro-optic behavior of liquid-crystal-filled silica opal photonic crystals: Effect of liquid-crystal alignment. *Phys. Rev. Lett.* **2001**, *86*, 4052–4055.

12. Ozaki, M.; Shimoda, Y.; Kasano, M.; Yoshino, K. Electric field tuning of the stop band in a liquid-crystal-infiltrated polymer inverse opal. *Adv. Mater.* **2002**, *14*, 514–518.

13. Mekis, A.; Chen, J.C.; Kurland, I.; Fan, S.; Villeneuve, P.R.; Joannopoulos, J.D. High transmission through sharp bends in photonic crystal waveguides. *Phys. Rev. Lett.* **1996**, *77*, 3787–3790.

14. Noda, S.; Tomoda, K.; Yamamoto, N.; Chutinan, A. Full three-dimensional photonic bandgap crystals at near-infrared wavelengths. *Science* **2000**, *289*, 604–606.

15. Srinivasan, K.; Painter, O. Momentum space design of high-Q photonic crystal optical cavities. *Opt. Express* **2002**, *10*, 670–684.

16. Akahane, Y.; Asano, T.; Song, B.-S.; Noda, S. High-Q photonic nanocavity in a two-dimensional photonic crystal. *Nature* **2003**, *425*, 944–947.

17. Dowling, J.P.; Scalora, M.; Bloemer, M.J.; Bowden, C.M. The photonic band edge laser: A new approach to gain enhancement. *J. Appl. Phys.* **1994**, *75*, 1896–1899.

18. Painter, O.; Lee, R.K.; Scherer, A.; Yariv, A.; O'Brien, J.D.; Dapkus, P.D.; Kim, I. Two-dimensional photonic band-gap defect mode laser. *Science* **1999**, *284*, 1819–1821.

19. Sakoda, K.; Ohtaka, K.; Ueta, T. Low-threshold laser oscillation due to group-velocity anomaly peculiar to two- and three-dimensional photonic crystals. *Opt. Express* **1999**, *4*, 481–489.

20. Foresi, J.S.; Villeneuve, P.R.; Ferrera, J.; Thoen, E.R.; Steinmeyer, G.; Fan, S.; Joannopoulos, J.D.; Kimerling, L.C.; Smith, H.I.; Ippen, E.P. Photonic-bandgap microcavities in optical waveguides. *Nature* **1997**, *390*, 143–145.

21. Notomi, M.; Kuramochi, E.; Taniyama, H. Ultrahigh-Q nanocavity with 1D photonic gap. *Opt. Express* **2008**, *16*, 11095–11102.

22. Tocci, M.D.; Bloemer, M.J.; Scalora, M.; Dowling, J.P.; Bowden, C.M. Thin-film nonlinear optical diode. *Appl. Phys. Lett.* **1995**, *66*, 2324–2326.

23. Hattori, T.; Tsurumachi, N.; Nakatsuka, H. Analysis of optical nonlinearity by defect states in one-dimensional photonic crystals. *J. Opt. Soc. Am.* **1997**, *14*, 348–355.

24. Dumeige, Y.; Vidakovic, P.; Sauvage, S.; Sgnes, I.; Levenson, J.A. Enhancement of second-harmonic generation in a one-dimensional semiconductor photonic band gap. *Appl. Phys. Lett.* **2001**, *78*, 3021–3023.

25. Ozaki, R.; Matsui, T.; Ozaki, M.; Yoshino, K. Electrically color-tunable defect mode lasing in one-dimensional photonic-band-gap system containing liquid crystal. *App. Phys. Lett.* **2003**, *82*, 3593–3595.

26. Ozaki, R.; Ozaki, M.; Yoshino, K. Defect mode switching in one-dimensional photonic crystal with nematic liquid crystal as defect layer. *Jpn. J. App. Phys.* **2003**, *42*, L669–L671.

27. Ozaki, R.; Moritake, H.; Ozaki, M.; Yoshino, K. Analysis of defect mode switching response in one-dimensional photonic crystal with a nematic liquid crystal defect layer. *J. App. Phys.* **2006**, *101*, doi:10.1063/1.2432877.

28. Ozaki, R.; Ozaki, M.; Yoshino, K. Defect mode in one-dimensional photonic crystal with in-plane switchable nematic liquid crystal defect layer. *Jpn. J. App. Phys.* **2004**, *43*, L1477–L1479.

29. Tagashira, K.; Yoshida, H.; Kubo, H.; Fujii, A.; Ozaki, M. Radial and azimuthal polarizer using a one-dimensional photonic crystal with a patterned liquid crystal defect layer. *Appl. Phys. Express* **2010**, *3*, doi:10.1143/APEX.3.062002.

30. Lin, Y.-T.; Chang, W.-Y.; Wu, C.-Y.; Zyryanov, V.Y.; Lee, W. Optical properties of one-dimensional photonic crystal with a twisted-nematic defect layer. *Opt. Express* **2010**, *18*, 26959–26964.

31. Hsiao, Y.-C.; Hou, C.-T.; Zyryanov, V.Y.; Lee, W. Multichannel photonic devices based on tristable polymer-stabilized cholesteric textures. *Opt. Express* **2011**, *19*, 23952–23957.

32. Hsiao, Y.-C.; Zou, Y.-H.; Timofeev, I.V.; Zyryanov, V.Y.; Lee, W. Spectral modulation of a bistable liquid-crystal photonic structure by the polarization effect. *Opt. Mater. Express* **2013**, *3*, 821–828.

33. Wei, L.; Alkeskjold, T.T.; Bjarklev, A. Compact design of an electrically tunable and rotatable polarizer based on a liquid crystal photonic bandgap fiber. *IEEE Photon. Technol. Lett.* **2009**, *21*, 1633–1635.

34. Safrani, A.; Abdulhalim, I. Liquid-crystal polarization rotator and a tunable polarizer. *Opt. Lett.* **2009**, *34*, 1801–1803.

35. Ye, Y.; He, S. 90° polarization rotator using a bilayered chiral metamaterial with giant optical activity. *Appl. Phys. Lett.* **2010**, *96*, doi:10.1063/1.3429683.

36. Yee, K.S. Numerical solution of initial boundary value problems involving Maxwell's equations in isotropic media. *IEEE Trans. Antennas Propag.* **1966**, *14*, 302–307.